Sustainable Drag Reduction in Turbulent Taylor-Couette Flows by Depositing Sprayable Superhydrophobic Surfaces

Siddarth Srinivasan, Justin A. Kleingartner, Jonathan B. Gilbert, and Robert E. Cohen*
Department of Chemical Engineering, Massachusetts Institute of Technology, 77 Massachusetts Avenue, Cambridge, Massachusetts 02139, USA

Andrew J. B. Milne and Gareth H. McKinley†
Department of Mechanical Engineering, Massachusetts Institute of Technology, 77 Massachusetts Avenue, Cambridge, Massachusetts 02139, USA

(Received 1 September 2014; revised manuscript received 15 November 2014; published 6 January 2015)

We demonstrate a reduction in the measured inner wall shear stress in moderately turbulent Taylor-Couette flows by depositing sprayable superhydrophobic microstructures on the inner rotor surface. The magnitude of reduction becomes progressively larger as the Reynolds number increases up to a value of 22% at $\mathrm{Re} = 8.0 \times 10^4$. We show that the mean skin friction coefficient C_f in the presence of the superhydrophobic coating can be fitted to a modified Prandtl–von Kármán–type relationship of the form $(C_f/2)^{-1/2} = M \ln(\mathrm{Re}(C_f/2)^{1/2}) + N + (b/\Delta r)\mathrm{Re}(C_f/2)^{1/2}$ from which we extract an effective slip length of $b \approx 19$ μm. The dimensionless effective slip length $b^+ = b/\delta_\nu$, where δ_ν is the viscous length scale, is the key parameter that governs the drag reduction and is shown to scale as $b^+ \sim \mathrm{Re}^{1/2}$ in the limit of high Re.

DOI: 10.1103/PhysRevLett.114.014501 PACS numbers: 47.85.lb, 47.27.N-, 68.08.Bc, 83.50.Rp

It is well known that superhydrophobic (SH) surfaces can reduce drag in laminar flows by presenting an effective wall slip boundary condition due to stable pockets of vapor within the asperities of the textured substrate [1,2]. The trapped vapor layer adjacent to the solid wall lubricates the fluid flow by introducing an effective slip boundary condition along portions of the wall, and consequently reduces the overall drag [3]. The magnitude of the effective slip length b in viscous laminar flows is governed by the surface feature length scale and the wetted solid fraction [4–6]. Measurements in various microchannel flows [7–11] yield values of b that are typically in the range of 10–30 μm.

There is less consensus on the extent to which microscopic effective slip can influence macroscopic skin friction in turbulent flows [12,13]. Numerical simulations of turbulent channel flows indicate that the shear-free liquid-vapor interface can reduce skin friction by introducing an effective slip velocity in the viscous sublayer [14,15], and by the suppression of turbulent flow structures in the near-wall region [16]. While recent experimental studies report varying amounts of drag reduction in turbulent flows using SH surfaces [17–19], there are inconsistencies in the magnitude of observed drag reduction across studies, and its dependence on the slip length, surface characteristics, and Reynolds number in turbulent flow remain unclear.

In this Letter, we demonstrate sustained reduction in frictional drag in turbulent Taylor-Couette (TC) flows by applying a polymeric SH coating to the inner rotor. The extent of drag reduction $\mathrm{DR} = 100 \times (\mathcal{T}^{\mathrm{flat}} - \mathcal{T}^{\mathrm{SH}})/\mathcal{T}^{\mathrm{flat}}$ based on the inner rotor torque $\mathcal{T}$, steadily increases with Re up to 22% at $\mathrm{Re} = 80\,000$. The reduction in friction arises from finite slip effects at the moving rotor. The two key results we describe in our Letter are (i) the magnitude of drag reduction is directly related to a dimensionless slip length $b^+ \equiv b/\delta_\nu$, which couples the effective slip length b to the viscous length scale $\delta_\nu = \nu/u_\tau = \nu\sqrt{\rho/\tau_i}$ of the turbulent flow (where ν is the kinematic viscosity, ρ is the liquid density, τ_i is the wall shear stress measured at the inner rotor and $u_\tau = \sqrt{\tau_i/\rho}$ is the friction velocity), and (ii) the proposal of a modified skin friction law from which a single value of b is obtained that accounts for the entire range of measured drag reduction for various Re.

The large gap TC apparatus [see Fig. 1(a)] has a rotating recessed end inner cylinder of radius $r_i = 14 \pm 0.01$ mm and stationary outer cylinder of radius $r_o = 34.3 \pm 0.1$ mm (so that $\eta = r_i/r_o = 0.41$; $\Delta r = r_o - r_i = 20.3$ mm). The recessed end traps a pocket of air inside the cavity [see Fig. 1(a)] to avoid end effects in torque measurements. The

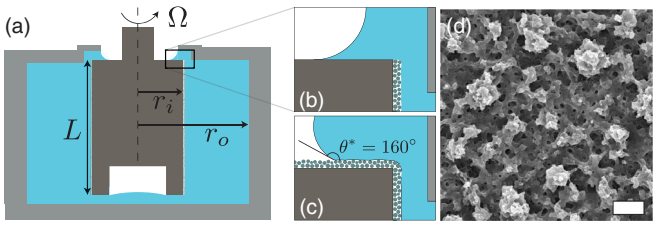

FIG. 1 (color online). (a) Cross-sectional view of the wide-gap Taylor Couette cell. (b),(c) The liquid seal with the plastron in the unconnected and connected state respectively. (d) SEM of the PMMA/FPOSS superhydrophobic surface spray-coated on the inner rotor. The scale bar corresponds to 50 μm.

height of the inner rotor was $L = 42.0 \pm 0.1$ mm, having an aspect ratio of $\zeta = L/(r_o - r_i) = 2.1$. The gap between the cylinders is filled with deionized water at 25 °C. The maximum rotation rate of the inner rotor was $\Omega_{\max} = 250$ rad/s, which represents a maximum attainable Reynolds number of $\mathrm{Re}_{\max} \equiv r_i \Omega_{\max} \Delta r/\nu = 8 \times 10^4$. This allows us to generate shear driven turbulent TC flows (past the Taylor vortex regime) [20,21], the onset of which occurs at a transition Reynolds number of $\mathrm{Re}_c \approx 1 \times 10^4$ for our system (for details, see the Supplemental Material [22]). We fabricated our SH surface on the inner rotor by spray coating a 50/50 (by weight) solution of poly (methyl methacrylate) (PMMA)/fluorodecyl polyhedral oligomeric silsesquioxane (FPOSS) at a concentration of $c = 50$ mg/ml, as described previously [27,28]. The coating was separately applied to produce either an unconnected configuration [Fig. 1(b)] where the trapped air (or "plastron") is isolated, or a connected configuration [Fig. 1(c)] in which the air layer is in continuous contact with an external air reservoir.

To quantify the initial wetted solid fraction, we extend the approach of Ref. [29] to enable *in situ* imaging of the plastron on a random textured SH surface using confocal microscopy, as detailed in the Supplemental Material [22]. In Fig. 2(a), we show the reconstructed 3D isosurface of the composite solid-liquid-air interface when a water drop (fluorescently labeled green), was deposited onto the SH coating (fluorescently labeled red). As expected, we observed that the liquid meniscus wets only on a fraction of the PMMA/FPOSS structures. The cut-away region reveals the unwetted (dry) PMMA/FPOSS structures beneath the liquid. Figure 2(b) shows an orthoslice of the spray coated texture and the liquid meniscus resting in the nonwetting state [30] along the AA' direction in Fig. 2(a). We determined the local height profile $h(x, y)$ of the PMMA/FPOSS and the vertical position of the liquid meniscus $z_0(x, y)$ from a series of these slices. Computing the averaged height-height correlation function [31] $H(r) = \langle (h(x' + r) - h(x'))^2 \rangle_{x,y}$ allows us to estimate a lateral correlation length, which corresponds to the size of the sprayed features, as $\xi = 15$ μm and a root-mean-square roughness $\omega = 8.5$ μm.

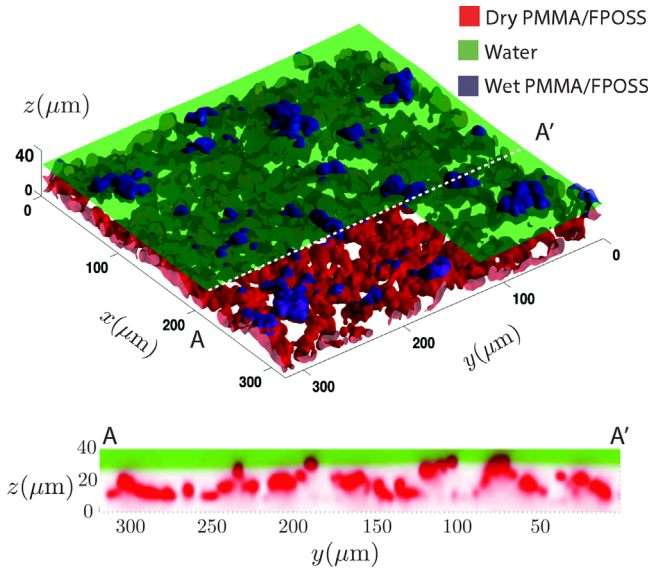

FIG. 2 (color online). (a) Reconstructed 3D isosurface from confocal microscopy of water (green) resting on PMMA/FPOSS structures (red) in the nonwetting state. (b) Superimposed fluorescence images of the PMMA/FPOSS structures (red) and the liquid meniscus (green) along the AA' slice plane.

In order to investigate the influence of the SH coating in turbulent TC flows, we systematically varied rotation rates to measure the global torque $\mathcal{T}$ on coated and uncoated rotors for $N = 17$ values of $\mathrm{Re} \in [1600, 80\,000]$. A single run consisted of either a ramp up in discrete steps from a minimum rate of $\Omega = 5$ rad/s ($\mathrm{Re} = 1600$) or a ramp down from the maximum $\Omega = 250$ rad/s ($\mathrm{Re} = 80\,000$). The torque $\mathcal{T}$ is measured over a period of 600 s at each Re. Viscous heating effects are negligible over this short time period (see Supplemental Material [22]). At least four replicates were performed for both the connected and unconnected state [see Fig. 1(b)]; the torque was averaged across all runs for each Re. In Fig. 3, we plot the averaged dimensionless torque $G = \mathcal{T}/(\rho \nu^2 L)$ for the various Re. For the uncoated inner rotor, where the relative standard deviation in the measured torque is $\sigma_r = 0.01$, we fit the measured torque to the predicted scaling $G \sim g(\eta)\mathrm{Re}^{5/3}$ for a turbulent TC flow in the wide-gap limit [32], as indicated by the dotted line in Fig. 3. While our best fit is in good agreement with the predicted exponent of 5/3, the value of $g(\eta) = 0.3$ that we obtained is smaller than the predicted value of $g(\eta) = [(1 + \eta)/2]/[\eta^{1/3}(1 - \eta)^2]$ from Ref. [32], suggesting that a very large gap width ($\eta < 0.5$) and small aspect ratio ($\zeta = 2.1$) influences the prefactor but not the torque scaling.

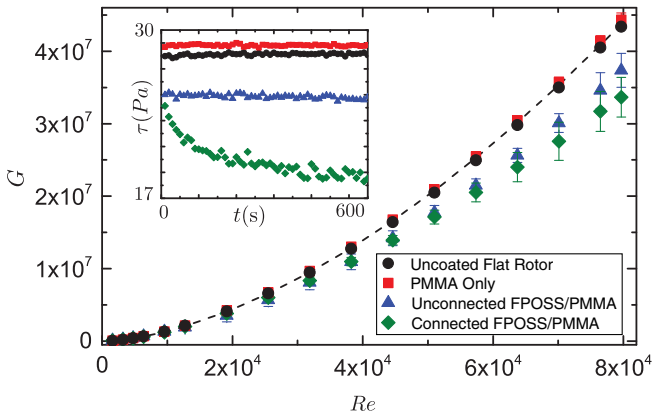

FIG. 3 (color online). Variation of the average dimensionless torque G against Re. The dotted black line represents the fit to the scaling $G \sim \mathrm{Re}^{5/3}$ from Ref. [32] for the uncoated rotor. Inset: Measurements of the dimensional inner wall shear stress τ against time for a fixed $\mathrm{Re} = 80\,000$ over 10 minutes.

Upon applying our PMMA/FPOSS coating onto the inner rotor, we consistently obtained a significant reduction in the measured torque for $\mathrm{Re} > \mathrm{Re}_c$. Remarkably, we found that the averaged drag reduction steadily increases with Re (see Fig. 3), from 6% at $\mathrm{Re} = 19\,000$ to a maximum of 15% at $\mathrm{Re}_{\mathrm{max}}$ for the unconnected configuration with an isolated plastron, and up to 22% at $\mathrm{Re}_{\mathrm{max}}$ in the case of the connected plastron. In the inset of Fig. 3, we plot the average inner wall shear stress $\tau_i = \mathcal{T}/(2\pi r_i^2 L)$ measured over a period of 600 s for a single measurement at $\mathrm{Re}_{\mathrm{max}}$. Initially, the rotor is at rest and is then accelerated to $\Omega = 250$ rad/s at $t = 0$. The measured torque reductions due to the superhydrophobic coating are 2 orders of magnitude larger than the ~0.02 Pa resolution limit of the sensor. The unconnected superhydrophobic coating shows a steady reduction of $\Delta\tau_i = 3.2$ Pa over the entire duration of the measurement. The connected configuration exhibits an additional decay in the measured torque with time, caused by the augmentation of air to the connected plastron at high rotor velocities, resulting in a final reduction in torque of $\Delta\tau_i = 8.0$ Pa in this configuration. Upon time averaging across multiple runs, we found larger relative deviations in the measured torque ($\sigma_r = 0.08$ at $\mathrm{Re}_{\mathrm{max}}$) for the SH coated rotor (see error bars in Fig. 3). In contrast, the PMMA-only coating does not support a plastron and drops of water deposited on the surface wet in the Wenzel state. Consequently, this surface shows a drag increase ($\Delta\tau_i = -0.7$ Pa) as a result of the increased wetted surface area that interacts with the turbulent flow. For a roughness amplitude of $k = 35$ μm [see Fig. 2(b)], the drag increase in the Wenzel state at the largest Re corresponds to a surface with dimensionless roughness $k^+ = k/\delta_\nu = 6.6$. In order to relate our measured drag reduction to effective slip phenomena, we apply a boundary layer theory to relate the global shear-stress measurements to Re. The dimensionless wall shear stress is typically expressed using a skin friction coefficient $C_f = \tau_i/(1/2\rho V_i^2) = 2(u_\tau/V_i)^2$. Here, $u_\tau = (\tau_i/\rho)^{1/2}$ is the friction velocity and $V_i = r_i\Omega$ is the inner rotor velocity for our TC system. In most shear driven turbulent flows, C_f is described either by a power law [32] or a semiempirical logarithmic law [20,21] expressed in Prandtl–von Kármán coordinates as

$$\sqrt{\frac{2}{C_f}} = M \ln\left(\mathrm{Re}\sqrt{\frac{C_f}{2}}\right) + N, \qquad (1)$$

where M and N are geometry-dependent constants that are analogous to the "universal" von Kármán constant κ and the additive constant B obtained for a perfect flat plate boundary layer [21]. The product $\mathrm{Re}(C_f/2)^{1/2}$ is identical to the friction Reynolds number $\mathrm{Re}_\tau \equiv u_\tau \Delta r/\nu$ which varies from $\mathrm{Re}_\tau \sim 480$–$3810$ in our system. Although the relative validity of the power-law theory compared to the logarithmic theory is still under dispute, empirical fits to the two forms are often indistinguishable [33]. In Fig. 4, we plot the measured skin friction coefficients for the flat, uncoated inner rotor as filled circles in Prandtl–von Kármán coordinates [34]. The solid line represents a linear regression of Eq. (1) applied to data points in the shear driven turbulent flow regime, (i.e., $\mathrm{Re} > \mathrm{Re}_c$), yielding values of $M = 3.9$ and $N = -11.7$. Deviations to the logarithmic skin friction law given by Eq. (1) are observable only when $\mathrm{Re} < \mathrm{Re}_c$ and the flow is still dominated by Taylor vortices [20,21]. To determine how Navier wall slip alters the skin-friction law given by Eq. (1) in our wall-bounded turbulent TC flow with a SH surface, we apply the angular momentum defect theory of Panton [35] and incorporate finite wall slip at the inner surface. Direct measurements of angular momentum profiles [36,37] as well as direct numerical simulations of turbulent TC flows [38] verify the existence of a core region with a weakly varying angular momentum dependence, as well as thin wall layers near the inner and outer cylinders that are characterized by a sharp decay in the angular momentum. Panton [35,39] asymptotically matches the expressions for the mean azimuthal momentum in the core region and the inner wall region to derive a logarithmic skin friction law of the form expressed in Eq. (1).

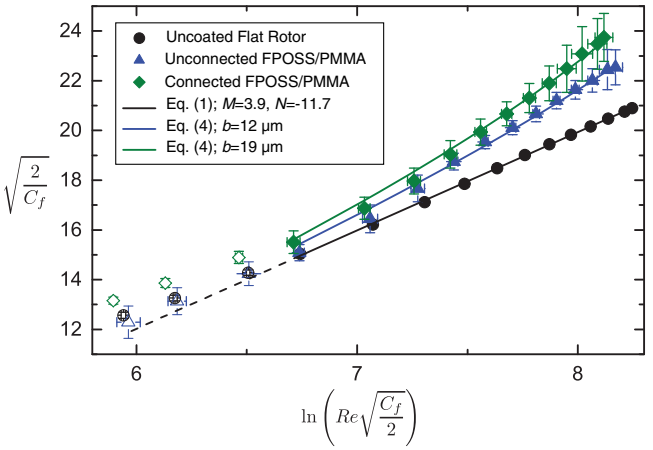

FIG. 4 (color online). Measured skin friction plotted in Prandtl–von Kármán coordinates. The solid black line is the fit to the logarithmic skin friction law given by Eq. (1) for $\mathrm{Re} > \mathrm{Re}_c$ with fitted values of $M = 3.9$ and $N = -11.7$. The solid blue and green curves are fits to Eq. (4) with $b = 12$ μm and $b = 19$ μm for the unconnected and connected SH surface, respectively.

We modify this theory by introducing a finite averaged slip velocity $\langle V_{\mathrm{slip}}\rangle$ that we relate to the local viscous stress at the inner rotor by the Navier slip hypothesis as $\langle V_{\mathrm{slip}}\rangle = b(d\langle V_\theta\rangle/dy)_{y=0}$, where b is the effective slip length due to the superhydrophobic coating and $(d\langle V_\theta\rangle/dy)_{y=0}$ is the time-averaged velocity gradient at the wall. In the immediate vicinity of the inner rotor, the slip velocities and angular momentum can be rescaled using inner variables defined in terms of the friction velocity u_τ and viscous length scale δ_ν. The distance away from the

inner rotor expressed in wall units is $y^+ = (r - r_i)/\delta_\nu$. If the velocity in the viscous sublayer close to the inner wall is shifted by a constant value according to Ref. [14], so that $\langle V_\theta^+ \rangle = y^+ + b^+$ and $d\langle V_\theta \rangle^+/dy^+ = 1$, the Navier-slip hypothesis upon scaling reduces to $V_{\text{slip}}^+ = b^+$, where $V_{\text{slip}}^+ = V_{\text{slip}}/u_\tau$ and $b^+ = b/\delta_\nu$. Following Ref. [35], we derive a skin-friction law that incorporates wall slip:

$$\frac{V_i}{u_\tau} = M \ln \text{Re}_\tau + N + b^+, \tag{2}$$

where M and N are the same geometry-dependent constants as in Eq. (1). Details of the derivation are provided in the Supplemental Material [22]. An additional simplification is introduced by assuming that the dimensional effective slip length b of the textured superhydrophobic surface is independent of the Reynolds number, so that, upon scaling

$$b^+ = \left(\frac{b}{\Delta r}\right) \text{Re} \sqrt{\frac{C_f}{2}}. \tag{3}$$

With this assumption of a constant physical slip length b in Eq. (2), and introducing C_f and Re in place of u_τ and Re_τ, we obtain a modified skin-friction law for turbulent flow that accounts for wall slip at a superhydrophobic surface and is of the form

$$\sqrt{\frac{2}{C_f}} = M \ln \left(\text{Re}\sqrt{\frac{C_f}{2}}\right) + N + \left(\frac{b}{\Delta r}\right) \text{Re} \sqrt{\frac{C_f}{2}}. \tag{4}$$

In Fig. 4, the measured values of C_f for the unconnected and connected SH surfaces are plotted in the Prandtl–von Kármán coordinates. The deviation of the SH data from the linear fit [Eq. (1) for the case of no slip] in Fig. 4 arises solely from the final term in Eq. (4). As the values of M and N were previously determined from the uncoated rotor, a nonlinear regression for the SH data using Eq. (4) results in values of $b = 12$ μm and $b = 19$ μm for the effective slip lengths of the unconnected and connected FPOSS coatings respectively. Therefore, a single value of the dimensional effective slip length is able to account for the entire range of drag reduction observed experimentally. The increasing values of b^+ and the larger values of drag reduction at higher Re are therefore a direct consequence of the smaller viscous length scale δ_ν in the flow. In the limit of $\text{Re} \to \infty$ we expect the logarithmic term in Eq. (4) to become much smaller than the final term for b^+ which varies linearly with $\text{Re}(C_f/2)^{1/2}$. Matching the left-hand side of Eq. (4) with this last term results in a predicted scaling of $C_f \sim 1/\text{Re}$, which in conjunction with Eq. (4) implies that $b^+ \sim \text{Re}^{1/2}$ at large Re. To verify this scaling, we compute the value of b^+ at each Re using the best-fit value of b (see Fig. 4) and the measured value of $\delta_\nu = \nu(\rho/\tau_i)^{-1/2}$. From Fig. 5, it is evident that b^+ indeed scales as $\text{Re}^{1/2}$ at large Re, for both the connected and unconnected SH surfaces. A similar scaling is expected for superhydrophobic drag reduction in turbulent boundary layer flows.

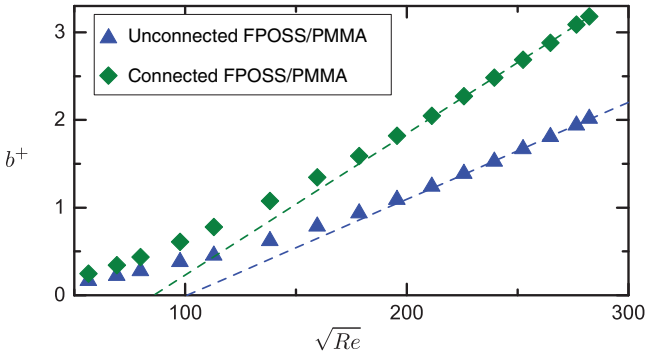

FIG. 5 (color online). Scaling of the dimensionless slip length $b^+ = b/\delta_\nu$ that is obtained using a fixed value of b from the nonlinear regression of Eq. (5) and with δ_ν determined from measurements of the Torque $\mathcal{T}$ at various Re. The dashed line is a fit to the scaling $b^+ \sim \sqrt{\text{Re}}$ for the last six data points.

In summary, we have demonstrated a reduction in the measured inner wall skin friction in turbulent TC flows by applying a sprayable SH surface onto the inner rotor. We observed that the extent of drag reduction increases with Reynolds number from 6% at $\text{Re} \sim 2 \times 10^4$ to a maximum of 15% and 22% for the isolated and connected plastrons, respectively, at $\text{Re} \sim 8 \times 10^4$. By applying a boundary layer theory for turbulent TC flow, we developed a modified form of the Prandtl–von Kármán skin friction law from which we extracted an effective slip length b that characterizes the connected and unconnected SH coatings and is consistent with earlier friction reduction measurements in viscous laminar flows. Our measurements demonstrate that the amount of drag reduction attainable in turbulent near-wall flows is directly related to the dimensionless effective slip length $b^+ = b/\delta_\nu$. As b^+ couples the effective slip length b (a material parameter) to the viscous length scale δ_ν of the turbulent flow, our results establish that superhydrophobic surfaces, despite typically exhibiting effective slip lengths of only tens of micrometers, can indeed reduce the skin friction in turbulent flows when the viscous sublayer is of comparable thickness, provided that the air plastron trapped in the SH surface can be stably maintained.

We would like to acknowledge D. Irvine for the use of the confocal microscope, J. Mabry for providing us with FPOSS, and J. Delannoy for assistance with calculating the Hurst exponent. We also wish to thank A. Mani, J. Kim, and M. Z. Bazant for helpful comments and discussions. This study was financially supported by the Office of Naval Research (ONR) through Contract No. 3002453814.

*recohen@mit.edu
†gareth@mit.edu

[1] A. Lafuma and D. Quéré, Nat. Mater. **2**, 457 (2003).
[2] J. P. Rothstein, Annu. Rev. Fluid Mech. **42**, 89 (2010).

[3] I. U. Vakarelski, J. O. Marston, D. Y. C. Chan, and S. T. Thoroddsen, Phys. Rev. Lett. **106**, 214501 (2011).
[4] C. Ybert, C. Barentin, C. Cottin-Bizonne, P. Joseph, and L. Bocquet, Phys. Fluids **19**, 123601 (2007).
[5] F. Feuillebois, M. Z. Bazant, and O. I. Vinogradova, Phys. Rev. Lett. **102**, 026001 (2009).
[6] K. Kamrin, M. Z. Bazant, and H. A. Stone, J. Fluid Mech. **658**, 409 (2010).
[7] J. Ou and J. P. Rothstein, Phys. Fluids **17**, 103606 (2005).
[8] R. Truesdell, A. Mammoli, P. Vorobieff, F. van Swol, and C. J. Brinker, Phys. Rev. Lett. **97**, 044504 (2006).
[9] P. Joseph, C. Cottin-Bizonne, J.-M. Benoît, C. Ybert, C. Journet, P. Tabeling, and L. Bocquet, Phys. Rev. Lett. **97**, 156104 (2006).
[10] C.-H. Choi and C.-J. Kim, Phys. Rev. Lett. **96**, 066001 (2006).
[11] C. Lee, C.-H. Choi, and C.-J. Kim, Phys. Rev. Lett. **101**, 064501 (2008).
[12] E. Aljallis, M. A. Sarshar, R. Datla, V. Sikka, A. Jones, and C.-H. Choi, Phys. Fluids **25**, 025103 (2013).
[13] M. Gad-el Hak, Phys. Fluids **25**, 079101 (2013).
[14] T. Min and J. Kim, Phys. Fluids **16**, L55 (2004).
[15] M. B. Martell, J. P. Rothstein, and J. B. Perot, Phys. Fluids **22**, 065102 (2010).
[16] H. Park, H. Park, and J. Kim, Phys. Fluids **25**, 110815 (2013).
[17] R. J. Daniello, N. E. Waterhouse, and J. P. Rothstein, Phys. Fluids **21**, 085103 (2009).
[18] B. Woolford, J. Prince, D. Maynes, and B. W. Webb, Phys. Fluids **21**, 085106 (2009).
[19] H. Park, G. Sun, and C.-J. Kim, J. Fluid Mech. **747**, 722 (2014).
[20] D. P. Lathrop, J. Fineberg, and H. L. Swinney, Phys. Rev. A **46**, 6390 (1992).
[21] G. S. Lewis and H. L. Swinney, Phys. Rev. E **59**, 5457 (1999).
[22] See Supplemental Material at http://link.aps.org/supplemental/10.1103/PhysRevLett.114.014501 for estimating the onset of shear driven turbulent TC flow, details of the confocal microscopy technique, the absence of viscous heating effects and the derivation of the skin friction law in the presence of slip [i.e., Eq. (2)], which includes Refs. [23–26].
[23] N. Otsu, IEEE Trans. Systems, Man, and Cybernetics **9**, 62 (1979).
[24] F. Bottiglione and G. Carbone, Langmuir **29**, 599 (2013).
[25] D. P. M. van Gils, S. G. Huisman, S. Grossmann, C. Sun, and D. Lohse, J. Fluid Mech. **706**, 118 (2012).
[26] J. Kestin, M. Sokolov, and W. A. Wakeham, J. Phys. Chem. Ref. Data **7**, 941 (1978).
[27] S. Srinivasan, S. S. Chhatre, J. M. Mabry, R. E. Cohen, and G. H. McKinley, Polymer **52**, 3209 (2011).
[28] S. Srinivasan, W. Choi, K.-C. Park, S. S. Chhatre, R. E. Cohen, and G. H. McKinley, Soft Matter **9**, 5691 (2013).
[29] P. Papadopoulos, L. Mammen, X. Deng, D. Vollmer, and H.-J. Butt, Proc. Natl. Acad. Sci. U.S.A. **110**, 3254 (2013).
[30] A. B. D. Cassie and S. Baxter, Trans. Faraday Soc. **40**, 546 (1944).
[31] M. Pelliccione and T.-M. Lu, in *Evolution of Thin Film Morphology*, Materials Science Vol. 108 (Springer, New York, 2008), pp. 29–46.
[32] B. Eckhardt, S. Grossmann, and D. Lohse, J. Fluid Mech. **581**, 221 (2007).
[33] W. K. George, Phil. Trans. R. Soc. A **365**, 789 (2007).
[34] P. S. Virk, D. C. Sherman, and D. L. Wagger, AIChE J. **43**, 3257 (1997).
[35] R. L. Panton, C. R. Acad. Sci. **315**, 1467 (1992).
[36] M. Burin, E. Schartman, and H. Ji, Exp. Fluids **48**, 763 (2010).
[37] G. P. Smith and A. A. Townsend, J. Fluid Mech. **123**, 187 (1982).
[38] S. Dong, J. Fluid Mech. **587**, 373 (2007).
[39] R. L. Panton, Phil. Trans. R. Soc. A **365**, 733 (2007).